TU Delft

Delft University of Technology

Fatigue resistance of rib-to-deck welded joint in OSDs, analyzed by fracture mechanics

Wu, Weijian; Kolstein, Henk; Veljkovic, M.

DOI
10.1016/j.jcsr.2019.105700

Publication date
2019

Document Version
Final published version

Published in
Journal of Constructional Steel Research

Citation (APA)
Wu, W., Kolstein, H., & Veljkovic, M. (2019). Fatigue resistance of rib-to-deck welded joint in OSDs, analyzed by fracture mechanics. *Journal of Constructional Steel Research*, *162*, Article 105700. https://doi.org/10.1016/j.jcsr.2019.105700

Important note
To cite this publication, please use the final published version (if applicable).
Please check the document version above.

Copyright
Other than for strictly personal use, it is not permitted to download, forward or distribute the text or part of it, without the consent of the author(s) and/or copyright holder(s), unless the work is under an open content license such as Creative Commons.

Takedown policy
Please contact us and provide details if you believe this document breaches copyrights.
We will remove access to the work immediately and investigate your claim.

This work is downloaded from Delft University of Technology.
For technical reasons the number of authors shown on this cover page is limited to a maximum of 10.

Green Open Access added to TU Delft Institutional Repository

'You share, we take care!' – Taverne project

https://www.openaccess.nl/en/you-share-we-take-care

Otherwise as indicated in the copyright section: the publisher is the copyright holder of this work and the author uses the Dutch legislation to make this work public.

Journal of Constructional Steel Research 162 (2019) 105700

Contents lists available at ScienceDirect

Journal of Constructional Steel Research

Fatigue resistance of rib-to-deck welded joint in OSDs, analyzed by fracture mechanics

Weijian Wu *, Henk Kolstein, Milan Veljkovic

Steel and Composite Structures, Department of Engineering Structures, Faculty of Civil Engineering and Geosciences, Delft University of Technology, P.O. Box 5048, 2600GA Delft, The Netherlands

ARTICLE INFO

Article history:
Received 24 March 2019
Received in revised form 15 July 2019
Accepted 16 July 2019
Available online xxxx

Keywords:
Rib-to-deck welded joint
Fracture mechanics
Geometric correction factors
Probabilistic analysis
Initial cracks
Weld profiles

ABSTRACT

The orthotropic steel decks (OSDs) are widely used in bridge engineering to support traffic loads. A possible crack, initiating from the weld toe of rib-to-deck welded joint and growing into the deck plate, is studied using linear elastic fracture mechanics. A detailed FE model is created and the results are compared with the fatigue tests published. Good agreement is found between beach marks from experiments and calculated crack fronts in FE. An engineering approach with the crack shape simplified as a semi-ellipse is applied. Geometric correction factors for a hand calculation method is proposed based on the parametric analysis. Using the proposed correction factors, Monte Carlo simulation is carried out with failure criteria defined with respect of the crack depth reaching "50%" of the deck thickness, "75%" of the deck thickness, and the failure criterion "2A FAD" according to BS7910. Predicted results using the failure criterion "75%" show good agreement with experimental data, for 5%, 50%, and 95% survival probabilities. Effects of initial crack shapes and sizes are discussed using the improved hand calculation model. Lower fatigue resistance is found when the initial crack is shallow or large. In addition to the standard weld geometry in which the weld profile is represented by a straight line, concave and convex arc shape weld profiles are studied. Fatigue resistance is improved in the case with assumption of concave arc weld profile. The difference of fatigue resistance between the cases with a straight line and convex arc weld profiles is small.

© 2019 Published by Elsevier Ltd.

1. Introduction

The traffic load is supported by deck plates in super structures of a bridge. One of the most common deck plate types is the orthotropic steel deck (OSD). It is widely used in long-span and movable bridges. The optimization target in design was to improve the ratio of load resistance to self-weight. This leads to high stress ranges under traffic loading, especially at welded joints. A lack of attention to the fatigue design of the deck in the past resulted in high maintenance cost today. Numerous fatigue cracks have been found in the deck plates. Typical cracks may appear at the rib-to-deck welded joint as shown in Fig. 1b. High stress arises in the welded area under local wheel loading. Cracks may appear from weld toe (cracks 1 and 4) or weld root (cracks 2 and 3) of the joint and grow through the deck plate (cracks 1 and 2) or the rib thickness and weld throat (cracks 3 and 4). This paper focuses on the analysis of the crack 1.

With a large amount of fatigue tests for OSDs carried out in the past four decades [2–10], the relationship between fatigue life and stress ranges (SN curves [11–13]) is developed to enable the fatigue design of the deck. By using the nominal stress approach, structural hot spot stress approach, or effective notch stress approach together with the corresponding pre-defined detail category [14], the fatigue life under traffic loading can be calculated.

It is important to understand the behaviour of crack propagation in existing bridges. Therefore, fracture mechanics which is used for crack propagation calculation becomes attractive. Suitable repair and inspection plans can be made based on the assessment of the current crack state and prediction of the crack growth. In addition to its application in aerospace and mechanical engineering, it is an interesting tool to analyze the structures in civil engineering [15,16]. Aygul [17,18] studied the 3D crack propagation under constant and variable amplitude loading of the weld toe in distortion-induced situation. Brighenti [19] reviewed the assessment of surface crack propagation under fatigue loading using fracture mechanics. Nagy [20] carried out case studies of an existing OSD bridge in Belgium using XFEM. Sanches [21] and Correia [22] carried out a probabilistic analysis for crack initiation and propagation of riveted and notched joints, respectively. Lukic [23] and Maljaars [24] applied probabilistic fracture mechanics to analyze the fatigue resistance of welded joints.

The state of a crack tip can be described by the stress intensity factors using fracture mechanics for the crack propagation analysis [25]. After obtaining the material properties, the crack propagation rate (da/dN) can be calculated by Paris' law [26]. Total fatigue life can therefore be

* Corresponding author.
E-mail address: W.Wu-1@tudelft.nl (W. Wu).

https://doi.org/10.1016/j.jcsr.2019.105700
0143-974X/© 2019 Published by Elsevier Ltd.

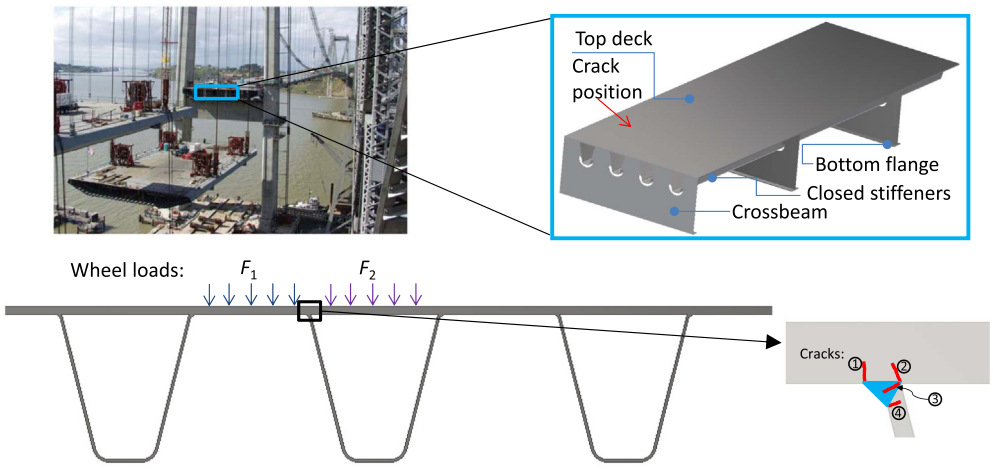

Fig. 1. Sketch of an orthotropic steel deck and rib-to-deck cracks (the photo of the bridge in construction is reprinted from the "FHWA" report with permission [1]).

predicted. The stress state of a crack tip can be calculated using either analytical solutions or numerical methods. The numerical approach is more suitable to solve the problems with complex geometric and stress conditions. The J-integral [27] or M-integral [28] can be numerically calculated by using a contour integral [29,30]. Within linear elastic fracture mechanics frame, the stress intensity factors can be easily obtained by these integrals. In order to provide quick engineering assessment, typical cases have already been analyzed by finite element (FE) method. The simplified hand calculation equations are proposed in guidelines, see BS7910 [31]. However, the rib-to-deck welded joint is currently not pre-qualified in design standards.

An advanced FE model is created following the specimen and set-up used in the experiments carried out by Nagy [20]. Using multi-point extrapolation method, the growth of a crack is predicted by the FE model. Using a simplified semi-ellipse shape crack, a parametric analysis is carried out. Geometric correction factors are developed for the empirical equations proposed by Newman et al. [32]. A probabilistic analysis carried out using Monte Carlo sampling technique successfully predicts the results from experiments with load ratios −1 and 0 [8–10,20,33–35].

2. Finite element model

2.1. Geometry of the specimen

The rib-to-deck welded joint can be loaded by a local wheel at the positions F_1 and F_2 as shown in Fig. 1. The deformation and stress state in the welded region are affected mainly by the loading positions and constraints of the deck plate nearby. A specimen containing one longitudinal stiffener with suitable boundary conditions is used in the experiments to simulate a complete OSD.

The 15 mm thick deck plate is stiffened by a 6 mm thick longitudinal closed stiffener as shown in Fig. 2. The cross section characteristics are taken from Nagy's thesis [20]. The detail simplified with 100% penetration is used for the FE analysis in the current paper. The trapezoidal stiffener with upper width 300 mm, lower width 150 mm, height 275 mm, and chamfer radius 24 mm is used. On the left and right hand side, the extended widths of the plate are 150 mm and 300 mm, respectively.

2.2. Loading and boundary conditions

In Fig. 2, the set-up is designed with clamping constraints on the left hand side using bolted connections and simple support on the right hand side using rolled plates. Cyclic loading is applied by the hydraulic actuator connected to the deck plate by using steel plates with the load ratio −1 or 0. The main purpose of the fatigue test is to study crack propagation under cyclic loading. Different amplitude load ranges are applied which result in the visible marks ("the beach marks") in the fracture surface because the crack growth rates are different when load ranges are changed.

A 3D finite element model, see Fig. 3, is created by the commercial software package "Abaqus 6.14-1" [29] with the dimensions, loading, and boundary conditions shown in Fig. 2. The load range 31 kN

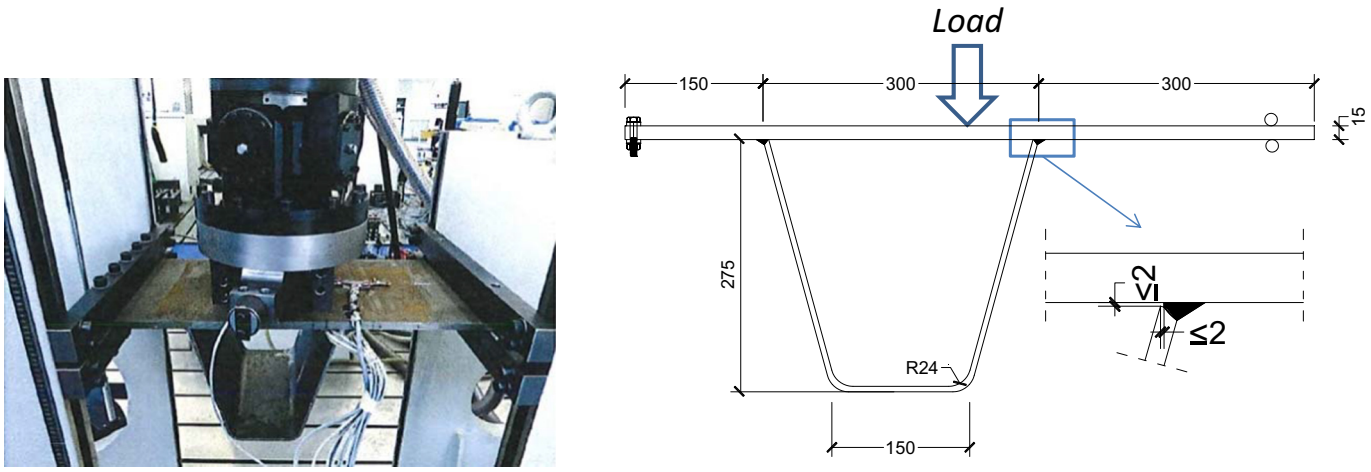

Fig. 2. The photo and sketch of the specimens and set-ups for "beach mark" tests [20] (unit: mm).

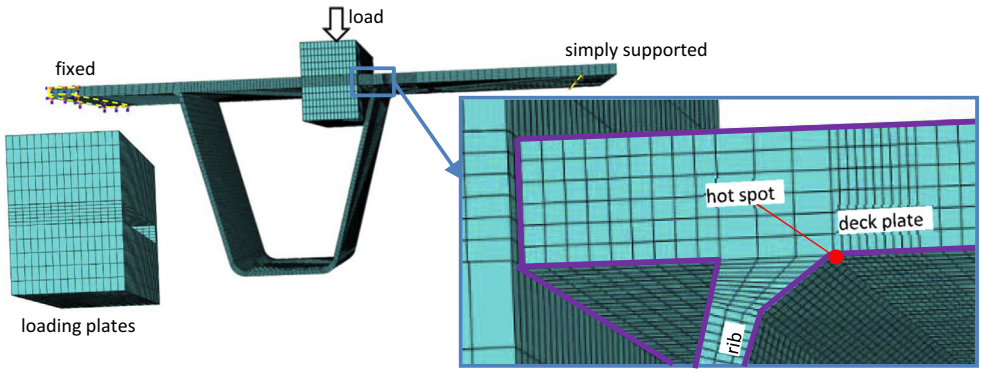

Fig. 3. FE model without crack.

(minimum 0 kN and maximum 31 kN) is applied on the FE model following specimen 10 (S10) in Nagy's thesis [20]. For the interaction of loading plates and deck, the "hard contact" is used in the normal direction and "penalty function" with friction coefficient 0.3 in the tangential direction [29]. A gap of 0.25 mm is defined between the loading plates and specimen in the FE models.

2.3. Crack insert

A crack is included at the weld toe position, perpendicular to the bottom surface of the deck plate. A half part of the crack with a depth a and a half length c is shown in Fig. 4a.

2.4. Meshing and element types

The specimen is fabricated from structural steel Grade S355 which is considered as a linear elastic material with Young modulus (E) and Poisson's ratio (ν) 210 GPa and 0.3, respectively. 20-node quadratic brick element "C3D20" is used for the specimen which is suitable to model a local stress concentration of linear elastic materials [29].

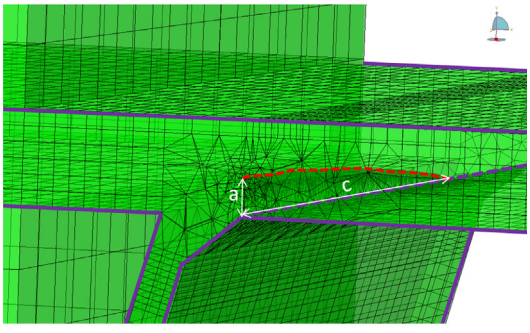

(a) Position of cracks (half view)

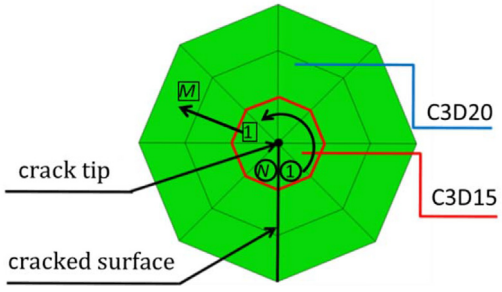

(b) Elements around the crack tip in the cross section

Fig. 4. FE model with initial crack.

8-node linear brick element "C3D8" is applied for the loading system to reduce the computational cost [29].

When the crack is introduced into the model, a sub part is selected in the software "FRANC3D" [30] which is meshed by 10-node quadratic tetrahedron element "C3D10" and will be remeshed during the crack propagation based on the inserted crack. Around the crack front, a part of FE mesh is modeled by "one ring" of "C3D15"(15-node quadratic triangular prism element) and two"adjacent rings" of "C3D20" [29], see Fig. 4b. The 3-circle elements are used to calculate the M-integral. In Fig. 5, the sketch of elements used in the FE models is shown.

2.5. Stress intensity factors calculation

Stress intensity factors can be calculated using M-integral for a mixed-mode problem. Different equilibrium states need to be used in the analysis. A relationship between J-integrals and M-integral is shown by Eqs. (1) and (2). The superscripts "1" and "2" represent two independent equilibrium states, and the superposition of two states is a new equilibrium state "0" [28]. In finite element calculation, the M-integral can be calculated by Eq. (3).

According to Yau [28] and Warzynek [36], stress intensity factors, K_{I}, K_{II}, and K_{III}, can be calculated via the M-integral using Eq. (4). Parameter A_q is the area of virtual extension along the crack front and superscripts 2a, 2b, 2c represent fracture modes I, II, and III, respectively. It should be noted that when the crack is at the surface, $(1-\nu^2)/E$ needs to be replaced by E due to the change from plane strain to plane stress condition.

$$J^{(0)} = J^{(1)} + J^{(2)} + M^{(1,2)} \tag{1}$$

where

$$M^{(1,2)} = \int_{\Gamma}\left(W^{(1,2)}ds - \left[T_i^{(1)}\frac{\partial u_i^{(2)}}{\partial x} + T_i^{(2)}\frac{\partial u_i^{(1)}}{\partial x}\right]ds\right) \tag{2}$$

in which $W^{(1,2)}$ is the mutual potential energy density of the elastic body, $T_i^{(1)}$ and $T_i^{(2)}$ are the surface tractions, $u_i^{(1)}$ and $u_i^{(2)}$ are the displacement vectors [28]. Γ is an arbitrary path close to the crack tips. Origin of the coordinate system locates at the crack tip. ds and ∂x represent the differential of arc length along path Γ and the component in x axis direction, respectively.

$$M^{(1,2)} = \sum_{n=1}^{N}\sum_{m=1}^{3}[F_n H_m]\Delta S_n \tag{3}$$

in which F_n is the integral function, H_m is the weight coefficient of the Gaussian quadrature formula (m is the number of circles), and Δs_n is a segment of the integration path within nth element (n is the number

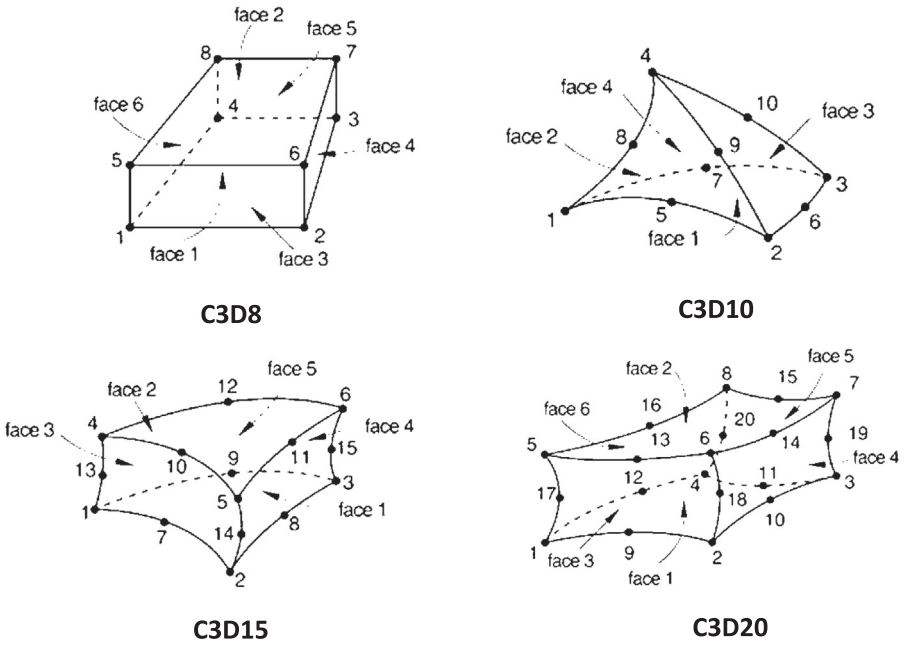

Fig. 5. Sketch of the elements used in the FE models [29].

of element in one ring) [28,36].

$$\begin{pmatrix} (1-\nu^2)/E & 0 & 0 \\ 0 & (1-\nu^2)/E & 0 \\ 0 & 0 & (1+\nu)/E \end{pmatrix} \begin{Bmatrix} K_{\mathrm{I}} \\ K_{\mathrm{II}} \\ K_{\mathrm{III}} \end{Bmatrix} = \begin{Bmatrix} M^{1,2a}/A_q \\ M^{1,2b}/A_q \\ M^{1,2c}/A_q \end{Bmatrix} \quad (4)$$

3. Numerical results

3.1. Evaluation of crack growth

When applying fracture mechanics approach to the fatigue life prediction, an initial crack needs to be included into the model as a starting point. The relationship of crack growth rate, da/dN, and the stress intensity factor range, ΔK, is empirically described by Paris' law, see Eq. (5) [26] where C and m are empirical material parameters obtained from experiments [25]. In this section, the threshold value $\Delta K_{threshold}$ is 63 N/mm$^{3/2}$, due to the high residual stress in the welded joints. The details can be found in Section 5.

$$\frac{da}{dN} = C(\Delta K)^m, \Delta K > \Delta K_{threshold} \quad (5)$$

In every increment, the crack growth at the deepest position, Δa_m is predefined. At other points, the crack increase is controlled by the relationship shown in Eq. (6) where C and m are set as 2.47×10^{-13} and 3.00 respectively based on the value in Nagy's thesis [20]. In Fig. 6, a sketch of this extrapolation is shown.

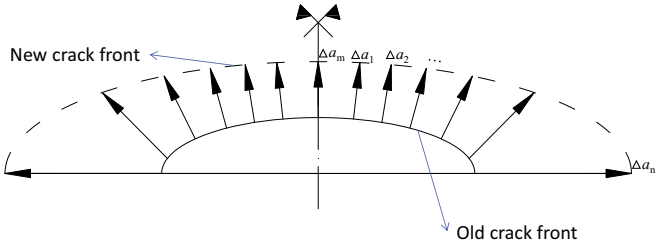

Fig. 6. Sketch of the crack propagation approach used in "FRANC3D" [30].

$$\Delta a_i = \Delta a_m \cdot \left(\frac{\Delta K_{eff,i}}{\Delta K_{eff,m}}\right)^m, i = 1 \ldots n. \quad (6)$$

Comparison of the calculated marks (solid green lines) and measured beach marks (dash black lines) of specimen 10 from Nagy's experiments [20] is shown in Fig. 7. Good agreement is found between FE calculation and experimental results both in the crack shapes and fatigue life. This indicates that applying Paris' law with ΔK from FE modelling to predict the fatigue crack propagation of the rib-to-deck welded joint is suitable. Intersection angle of the crack front and surface, θ, is small. A properly assumed crack from the beginning is important for the crack propagation simulation at the edges.

3.2. Stress intensity factor ranges along the crack front

Distribution of stress intensity factor ranges in mode I (ΔK_{I}) along the crack fronts at the 7 steps of calculation is shown in Fig. 8. In the beginning, maximum values are at the deepest positions ($\phi = \pi/2$) of crack fronts. When the crack depth a closes to the half thickness of the deck plate ($a = 7.06$ mm), ΔK_{I} increases faster at $\phi = 0.6\pi/2 = 0.94$. It indicates the change of the crack shape. ΔK_{I} at $\phi = \pi/2 = 1.57$ grows from 689 N/mm$^{3/2}$ to 748 N/mm$^{3/2}$ when a increases from 4.88 mm to 7.06 mm and then grows slowly till 8.88 mm. At $\phi = 0.6\pi/2 = 0.94$ the growth of 77 N/mm$^{3/2}$ and 84 N/mm$^{3/2}$ are found in the first four and the last three increments, respectively.

4. Geometric correction factors

It was shown that the crack extrapolated by multi-points using Paris' law can predict fatigue life and crack shapes well. It would be necessary to introduce a crack following the shape observed in the experiments. In current design codes like IIW recommendations and BS7910 [14,31], the surface crack shape is described by a depth a and a half length c of a semi-ellipse, see Fig. 9. In order to be consistent with engineering practice, all cracks defined in the following sections are based on this assumption for the sake of simplification. Only two points, the deepest and surface points, are used to identify the crack propagation. Similarly with the aforementioned approach, the depth increment a is

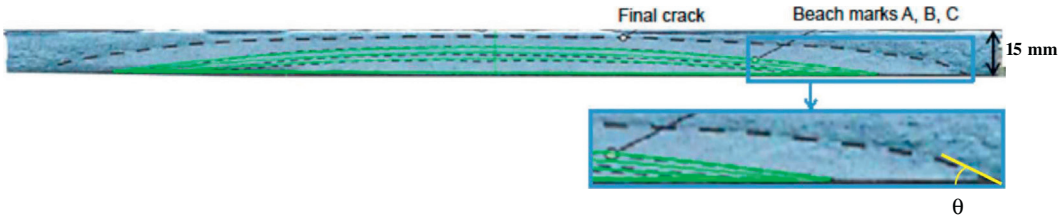

Fig. 7. Comparison of the calculated crack shapes (solid green lines) and beach marks (dash black lines) [20]. (For interpretation of the references to colour in this figure legend, the reader is referred to the web version of this article.)

pre-defined and corresponding fatigue life is calculated by Paris' law. The growth of the half length c can then be calculated. This approach is developed by "Newman and Raju" and gives a good prediction of semi-elliptical crack propagation under tension and bending loads [37]. Stress intensity factors are calculated by the empirical Eq. (7) [32].

It is necessary to correct the basic Eq. (7) [32] with the geometric correction factor M_k when different shapes of joints containing complex details are analyzed, see Eq. (9). For the rib-to-deck welded joint, the plate (deck) is strengthened by the longitudinal rib which causes the local stress concentration. In Eq. (9), ΔK_I is calculated based on M_k. Membrane (M_m) and bending (M_b) correction factors are separately treated for the semi-elliptical surface crack. In this case, bending stress is the dominant component at the cross section of the deck plate at weld toe of the rib-to-deck welded joint.

$$\Delta K_I = (M_m \Delta\sigma_m + M_b \Delta\sigma_b) \cdot \sqrt{\frac{\pi a}{Q}} \tag{7}$$

where $\Delta\sigma_m$ and $\Delta\sigma_b$ are the membrane and bending stress ranges, respectively. Q is the flaw shape parameter according to [32]:

$$Q = 1.0 + 1.464\frac{a}{c} \tag{8}$$

$$\Delta K_I = M_k(M_m(1-\Omega) + M_b\,\Omega)\Delta\sigma_{HSS}\sqrt{\frac{\pi a}{Q}} \tag{9}$$

Ω represents a proportion of the bending stress in structural hot spot stress range $\Delta\sigma_{HSS}$. The parameter Ω is set as 1 in the current paper.

In Sections 4.1 to 4.3, three types of weld profiles are considered, Type 1, Type 2, and Type 3 as shown in Fig. 10. Type 1 profile represents the most common assumption of the weld profile by using a straight line. Type 2 and Type 3 profiles replace the straight line by a concave and a convex arc to consider the favourable and unfavourable assumptions, respectively. Geometric correction factors (M_k) for calculation of the stress intensity factors based on these three types are obtained using the results from the FE modelling. For Type 2 profile, the strength of the weld throat may be weakened due to the removal of weld material. Research of that topic is left out of the scope of the current paper.

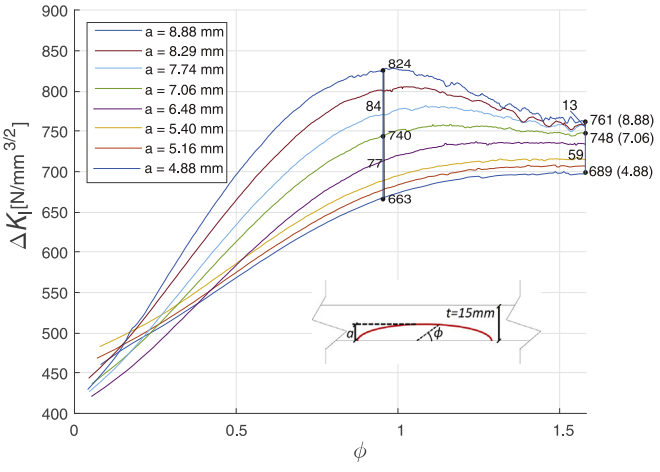

Fig. 8. Stress intensity factor ranges at crack fronts for the specimen 10 in Nagy's experiments [20].

4.1. Type 1 weld profile

Stress intensity factors along the crack front for Type 1 weld profile is calculated with different crack shapes (ratios $a/c = 0.067, 0.1, 0.2, 0.5$) and sizes a/t_{deck} (a/15 mm) in the range from 0.0067 to 0.73, where t_{deck} is the deck plate thickness. The values $c/a = 2, 5, 10, 15$ are originally used when inserting an initial crack in the FE models. To keep in line with the parameters in design codes, a/c is used in this paper. An increment of $a = 1.0$ mm is used for the crack $a > 1.0$ mm. For $a < 1.0$ mm, the increment of 0.1 mm is applied. The analysis is based on the FE model, see Fig. 3.

In Fig. 11, the normalized ΔK_I obtained at the load range 1 kN at three positions, $\phi = 0, \pi/4, \pi/2$, is shown based on the results from FE. The position $\phi = \pi/4$ is intentionally shown here for a comparison with the values at the surface, $\phi = 0$. ΔK_I increases with the crack size grows. A linear increase trend is shown when the relative crack depth a/t is between 0.1 and 0.5. At the positions $\phi = \pi/4$ and $\pi/2$, the values are rather close till a/t reaching 0.60 from where the ΔK_I starts to drop at $\phi = \pi/2$. At the surface, ΔK_I is smaller than at the positions $\phi = \pi/4$ and $\pi/2$.

The geometric correction factor M_k is calculated by dividing ΔK_I from FE calculation with $(M_m(1-\Omega) + M_b\,\Omega)\Delta\sigma_{HSS}\sqrt{\frac{\pi a}{Q}}$ according to Eq. (9). The results are plotted in Fig. 12 and the calculated results are described by fitted curves with dash lines.

Based on the calculated M_k, the hand calculation equations for the correction factor at the deepest crack point $M_{k,a}$ ($\phi = \pi/2$) and the surface edges $M_{k,c}$ ($\phi = 0$) can be proposed by fitting the FE results with the curves. In Fig. 13, two fitted curves are shown for $M_{k,a}$, the dash curve in cyan colour for the cracks with $a/c = 0.1$ and dash curve in blue colour for all the considered cracks. A small difference between the fitted curves is observed when $a/t < 0.1$. For $a/t > 0.1$, the curves containing all the data show slightly smaller values. For shallow cracks $a/c = 0.0667$, a clear drop is found when $a/t > 0.6$. It is explained as the effect

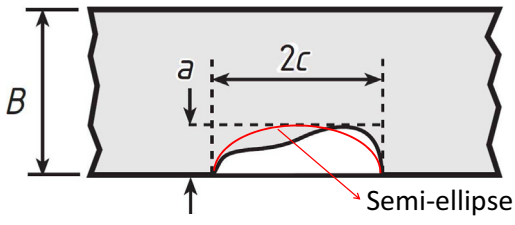

Fig. 9. Typical surface crack simplification in the design code BS7910 [31].

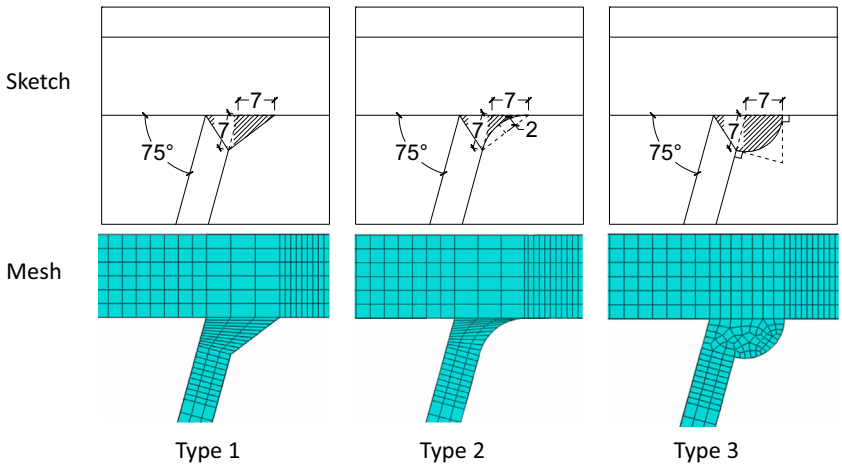

Fig. 10. Sketch of the weld profile used in the model (unit: mm).

of stress redistribution caused by the change in structural integrity with the propagation of cracks. The fitted curve in the case $a/c = 0.1$ is used for all the considered cases in the calculation of $M_{k,a}$. It is suitable because fatigue propagation period with small cracks dominates the total fatigue life. Fig. 14 presents FE results and fitted curves for $M_{k,c}$. For different crack shapes, the difference can be observed in small cracks. For instance, $a/c = 0.0667$ have higher $M_{k,c}$ when $a/t < 0.6$ and drop faster with the crack growth compared with the case $a/c = 0.1$. Moreover, the coefficient of determination is 0.7729, lower than the value 0.9793 in fitting $M_{k,a}$.

By introducing the geometric correction factor M_k, the calculation procedure using the fitted curves is given as follows. The calculation can be divided into two steps.

Firstly, the values of $M_{k,a}$ and $M_{k,c}$ with the crack shape $a/c = 0.1$ is calculated using Eq. (10). Correction factors are $M_{k,a}$ and $M_{k,c01}$ where subscript 01 means $a/c = 0.1$. For $M_{k,a}$, the subscript 01 is not written because it is assumed that the case with crack shape $a/c = 0.1$ represents all the considered cases.

Secondly, a crack shape correction factor, M_{sc}, is added to calculate $M_{k,c}$ using Eq. (11). Eq. (12) gives the formula for M_{sc}. A maximum difference ±0.12 of the deviation ($(M_{k,c,fitted} - M_{k,c,FE})/M_{k,c,FE}$) for the hand calculation by the fitted curves compared with FE results is shown in Fig. 15. The parameters, p_1 to p_5, of these fitted curves for calculating $M_{k,a}$ and $M_{k,c}$ are shown in Table. 1.

$$\begin{aligned} M_{k,a} &= p_1 \cdot e^{p_2 \cdot a/t} + p_3 \cdot e^{p_4 \cdot a/t} \\ M_{k,c01} &= p_1 \cdot e^{p_2 \cdot a/t} + p_3 \cdot e^{p_4 \cdot a/t} \end{aligned} \tag{10}$$

$$M_{k,c} = M_{sc} M_{k,c01} \tag{11}$$

in which:

$$M_{sc} = p_1 \cdot e^{\frac{-a/c}{p_2}} + p_3 \cdot e^{\frac{-a/t}{p_4}} + p_5 \cdot e^{\frac{-a/c}{p_2}} \cdot e^{\frac{-a/t}{p_4}} \tag{12}$$

4.2. Type 2 weld profile

Type 2 profile represents the favourable weld profile with smaller interaction angles between the base material and weld. Compared with Type 1 profile, $M_{k,a}$ at position $\phi = \pi/2$ is smaller with the values around 1 when the relative crack depth a/t is close to 0, see Fig. 16. It indicates that Type 2 profile effectively reduces the local stress

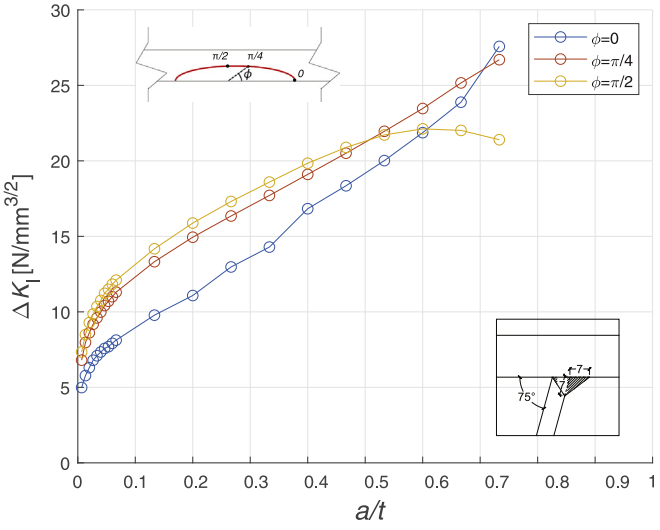

Fig. 11. ΔK_I under load range 1 kN with $a/c = 0.1$.

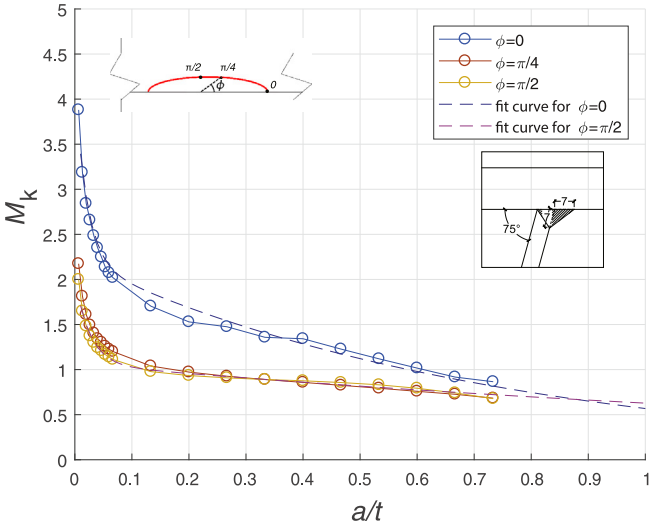

Fig. 12. Geometric correction factors at 3 positions with a/c = 0.1.

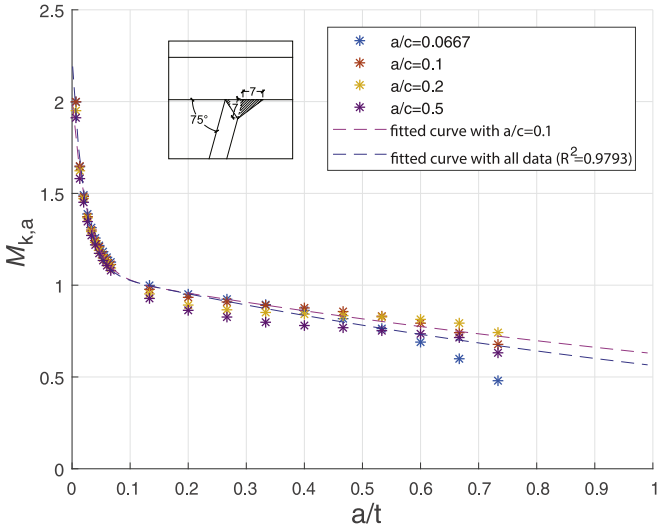

Fig. 13. Geometric correction factor $M_{k,a}$ with various crack shapes.

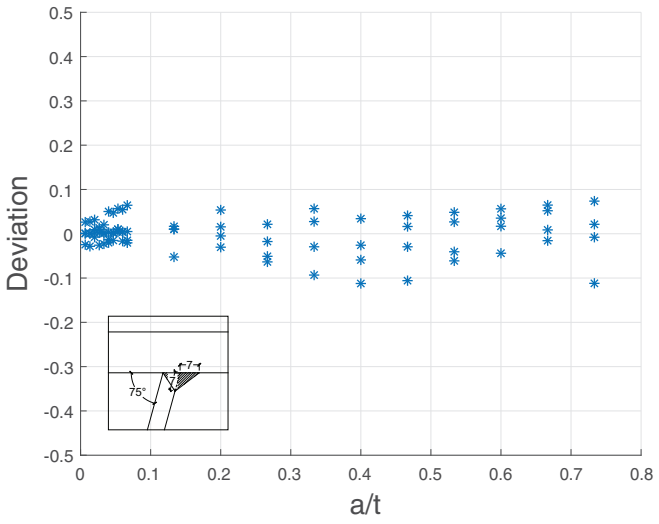

Fig. 15. Deviation of the hand calculation compared with FE results.

concentration at the weld toe and it is a beneficial weld profile for fatigue resistance. At position $\phi = 0$, $M_{k,c}$ is close to 1.3 and also drops with the increase of crack. In general, M_k changes linearly with the crack growth. The calculation of fitted curves follows Eqs. (12) and (13), and parameters are shown in Table. 1.

$$M_{k,a} = p_1 \cdot a/t + p_2$$
$$M_{k,c01} = p_1 \cdot a/t + p_2 \quad (13)$$

4.3. Type 3 weld profile

The correction factor M_k for Type 3 profile is shown in Fig. 17. The factor has a trend similar to Type 1 profile which shows large values when the cracks are small. Eqs. (10) and (12) are used for fitting the curves. The numerical values are shown in Table. 1.

In Fig. 18, correction factors for three types of cracks are compared. The values of $M_{k,a}$ are very close for Types 1 and 3 while the difference is slightly larger for $M_{k,c}$. As already discussed, Type 2 profile has smaller values compared with Types 1 and 3 weld profiles.

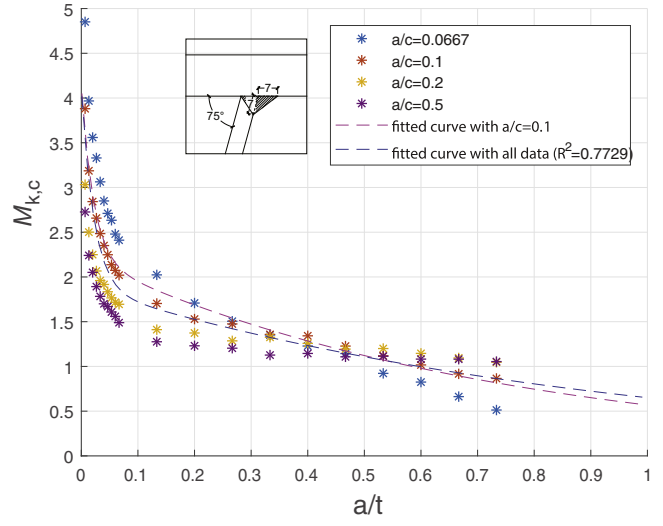

Fig. 14. Geometric correction factor $M_{k,c}$ with various crack shapes.

4.4. Validation with experiments

To verify the results of this simplified calculation, the specimen 10 in Nagy's thesis is used with the initial crack $a_0 = 0.13$ mm, $c_0 = 137.20$ mm, $C_a = 2.47 \times 10^{-13}$, $C_c = 5.21 \times 10^{-13}$, and $m = 3.00$ [20]. The definition of these parameters is given in Section 5.

In Fig. 19, the calculated crack depth, a, propagates exponentially with load cycles. The results show good agreement with experimental values. For the half length c, the calculated results grow slower compared with measured lengths from beach marks. This is understandable if we recall that the end angles θ in Fig. 7 are much smaller than the assumed $\theta = \pi/2$ which is the predefined values in the hand calculation model. Based on the crack propagation calculated by Eq. (6), a distance Δa_i is calculated to propagate the crack front at each point. The propagation direction is perpendicular to the old crack front. The growth of the half crack length Δc is $\Delta a_n / \sin(\theta)$. A small θ results in a smaller $\sin(\theta)$ and therefore a larger Δc. It should be noted that the increase of crack depth a dominates total fatigue life when the crack is so shallow. Accurate prediction of the crack depth a guarantees the fatigue life prediction.

In case that the geometric correction factor M_k is not applied in the calculation (dash lines), the crack propagation will be much slower, and therefore the fatigue resistance may be overestimated.

5. Probabilistic analysis

5.1. Fatigue life calculation

Probabilistic analysis is performed using Monte Carlo simulation for the crack initiating from the weld toe of the rib-deck welded joint in

Table 1
Parameters for fitting the geometric correction factors M_k.

Fitted	Type 1		Type 2		Type 3		Types 1, 2, 3
Constant	$M_{k,a}$	$M_{k,c01}$	$M_{k,a}$	$M_{k,c01}$	$M_{k,a}$	$M_{k,c01}$	M_{sc}
p_1	0.96	1.93	−0.47	−0.90	1.73	4.26	7.43
p_2	−38.26	−46.63	1.07	1.32	−60.97	−61.91	0.05
p_3	1.06	2.21	–	–	1.12	2.43	0.72
p_4	−0.53	−1.36	–	–	−0.65	−1.61	−1.36
p_5	–	–	–	–	–	–	−5.51
R-square	0.9936	0.9986	0.9900	0.9800	0.9919	0.9950	0.9551
Equation	10	10	13	13	10	10	12

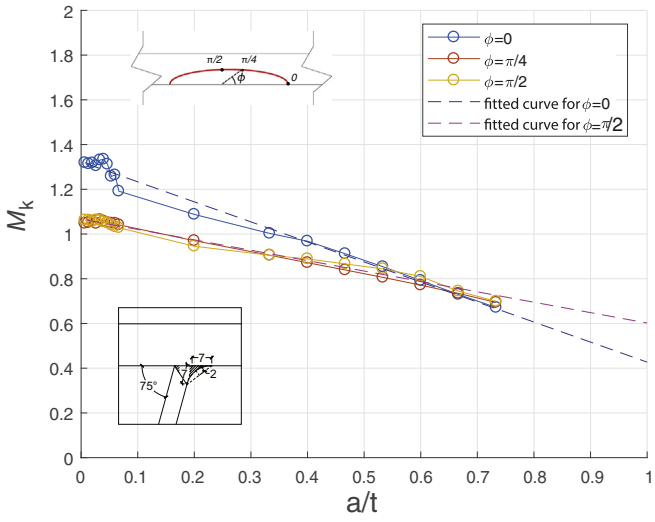

Fig. 16. Geometric correction factors at 3 positions with a/c = 0.1 of Type 2 profile.

OSDs. Fatigue life of the specimen is evaluated by the Paris' law, Eq. (5) [26], with different failure criteria (crack depth reaches "50%" of the deck plate thickness used by Lukic and Cremona [23], "75%" by IIW recommendations [14], and "2A FAD" in BS7910 [31]). Eq. (9) is applied to calculate stress intensity factor ranges with the M_k obtained as discussed in Section 4. According to Zerbst et al. [38], the secondary stresses (welding induced residual stress in this case) effect may be relaxed during crack propagation. Discussion of the secondary stress effect for the failure criterion is left out the scope of the current paper. Only primary stresses caused by an external load are considered in the "2A FAD" calculation in the current paper.

In the engineering analysis, the total fatigue life N_f is divided into the crack initiation period N_i and the crack propagation period N_p, see Eq. (14). When the crack can be observed by eye or the strain distribution is affected, the stage is defined as the end of crack initiation. However, small flaws may be induced in the material during the manufacturing or fabrication process. For welded structures, these initial flaws are heavily affected by the welding procedure and cooling conditions. Welded joints contain larger imperfection than the base material. A conservative way to calculate the fatigue life of welded structures is to assume that the propagation of the small flaw is equal to the total

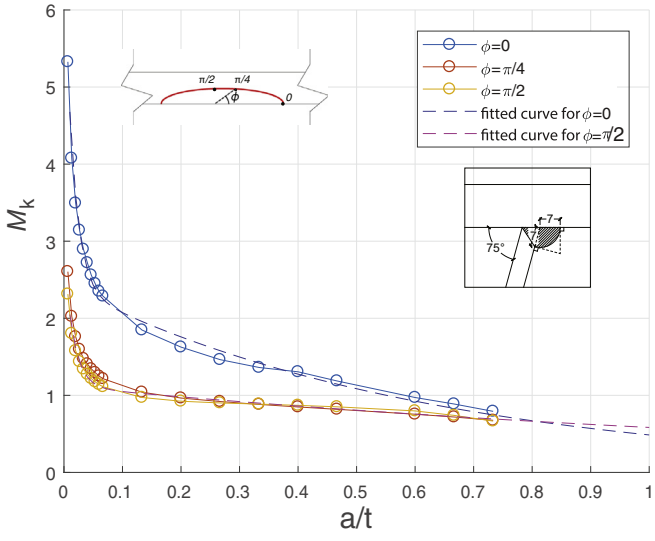

Fig. 17. Geometric correction factors at 3 positions with $a/c = 0.1$ of Type 3 profile.

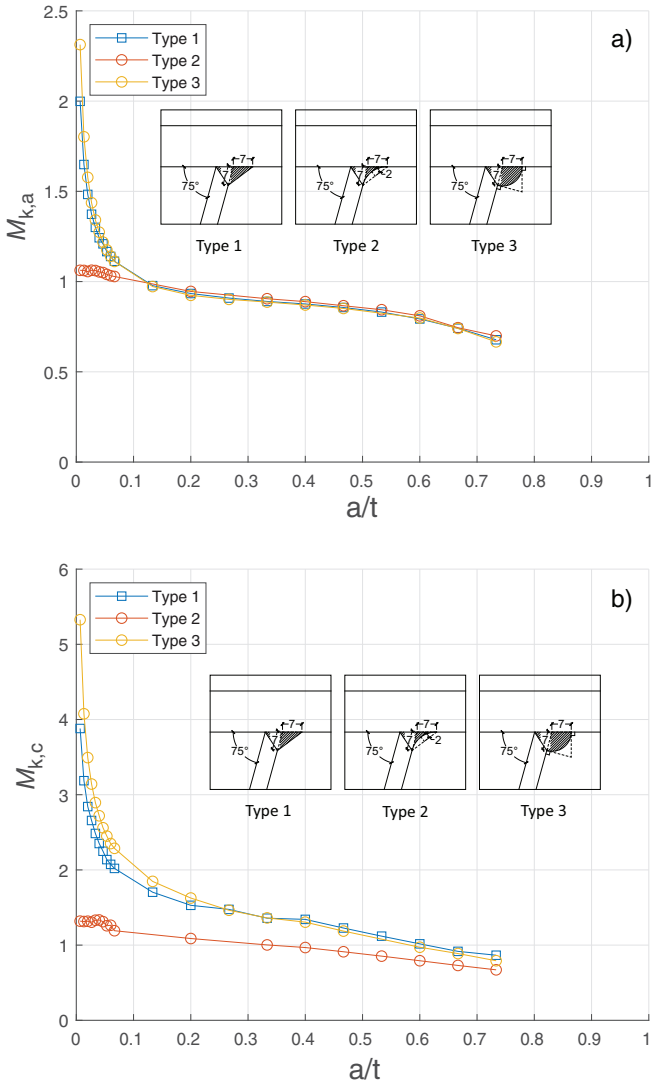

Fig. 18. Comparison of geometric correction factor M_k with $a/c = 0.1$ in 3 details. a) values for the deepest point ($M_{k,a}$), b) values for the surface edges ($M_{k,c}$).

fatigue life (N_f). This assumption is used in the current paper for the Monte Carlo simulation based on linear elastic fracture mechanics.

$$N_f = N_i + N_p \tag{14}$$

5.2. Parameters of probabilistic distributions

Table 2 lists the probabilistic density functions and the input variables used in the Monte Carlo simulation. The explanation of numerical values is shown:

5.2.1. Initial crack depth a_0

Initial cracks in welded structures may originate from notches caused by fabrication procedure. The sizes can range from grain scale to several millimeters. The mean value $a_0 = 0.1$ mm is proposed by IIW recommendations [14] and has been proved to be suitable for many cases. The IIW recommendations don't give the Coefficient of Variation (CoV), therefore Lognormal density function with the mean value $a_0 = 0.11$ mm and CoV 1.00 are used following the findings in the EU Report "BriFaG" [39].

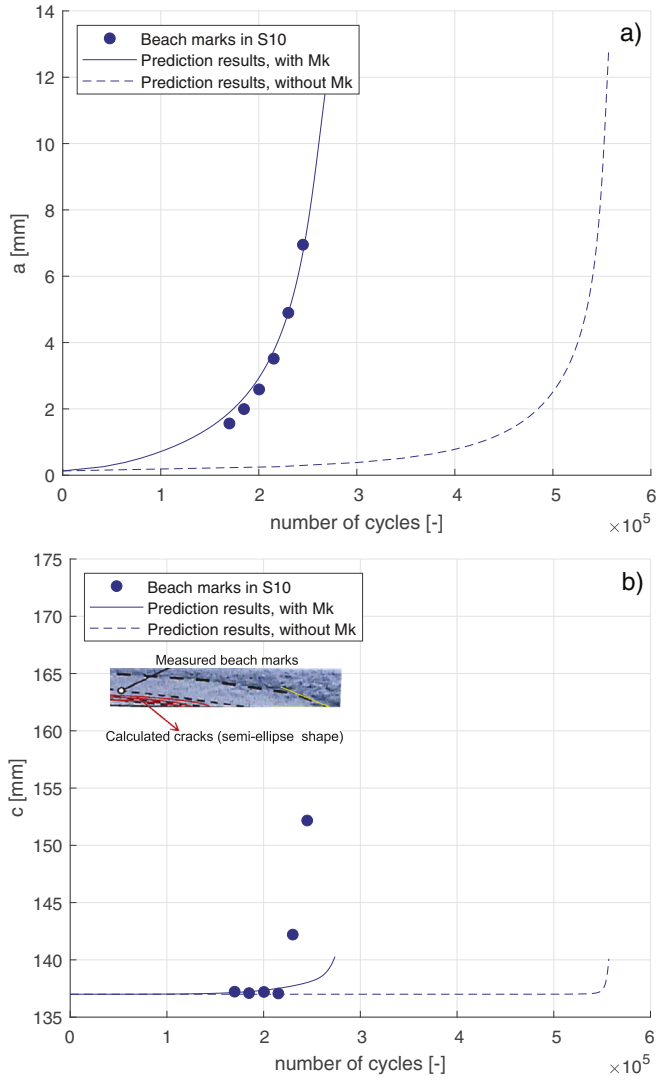

Fig. 19. Comparison of beach marks in the S10 from experiment [20] and hand calculation.

5.2.2. Initial crack shape a_0/c_0

Various crack shapes exist in welded joints ranging from 0 to 1 with structural details, crack depths, and applied stresses [23]. Under bending stress, it is recommended to use $a_0/c_0 = 0.10$ as the mean value by IIW recommendations [14], and the CoV 0.41 is taken from the paper of Lukic and Cremona [23].

Table 2
Variables and probabilistic functions for the Monte Carlo simulation.

Variable	Density function	Mean value	CoV
a_0	Lognormal	0.11 [39]	1.00 [39]
a_0/c_0	Lognormal	0.10 [14]	0.41 [23]
C_a $(R = -1)$	Lognormal	1.00×10^{-13} [24]	0.98 [24]
C_a $(R = 0)$	Lognormal	5.21×10^{-13} [24]	0.98 [24]
C_c	Lognormal	5.21×10^{-13} [24]	0.98 [24]
m	Deterministic	3.00 [14]	–
$\Delta K_{threshold}$ $(R = -1)$	Lognormal	170.00 [24]	0.20 [24]
$\Delta K_{threshold}$ $(R = 0)$	Lognormal	63.00 [14]	0.40 [39]
σ_y	Lognormal	350.00 [39]	0.07 [39]
σ_u [a]	Lognormal	525.00 [39]	0.07 [39]
B_{HSS}	Lognormal	1.00 [39]	0.05 [39]
K_{mat}	Weibull	2250.00 [39]	0.25 [39]

Notes: Units in N and mm.
[a] $\sigma_u = 1.5 \cdot \sigma_y$.

5.2.3. Paris' law parameters C,m, and $\Delta K_{threshold}$

Material parameters C and m are often analyzed with Lognormal and Deterministic distribution, respectively [39]. The value of m is set as 3.00 following IIW recommendations [14] which is the same as the slope of SN curves for normal stress. Parameter C is affected by micro structures of material and the applied stresses. The load ratio (R) can affect its stress situation and therefore the values of C. Residual stress induced by welding is hard to be assumed without knowing the details of welding process and constrains conditions during welding. In the current paper, 2 load ratios $R = -1$ and 0 are included in Monte Carlo simulation. The values of material parameters C_a and C_c are taken from Maljaars et al. [24] which are obtained based on the experiments using the steel plate cut from the OSD. The threshold value of stress intensity factor range $\Delta K_{threshold}$ is also lognormally distributed and influenced by the load ratio. The mean value 63 N/mm$^{3/2}$ is used for $R = 0$ following IIW recommendations [14], and 170 N/mm$^{3/2}$ for $R = -1$ from the findings in Maljaars et al. [24].

5.2.4. Structural steel property σ_y and σ_u

Structural steel Grade S355 is considered with the yield stress 350 MPa distributed in Lognormal density function with CoV of 0.07 and the ultimate stress assumed as 1.5 times of yield value following the values used in the report "BriFaG" [39].

5.2.5. Structural hot spot stress deviation ratio B_{HSS}

The structural hot spot stress range $(\Delta\sigma_{HSS})$ is obtained by extrapolation from the recommended surface points to the hot spots to consider the stress concentration. The deviation between the actual and calculated $\Delta\sigma_{HSS}$ can be considered by $B_{HSS} \cdot \Delta\sigma_{HSS}$ where the ratio B_{HSS} is Lognormal distributed according to the report "BriFaG" [39].

5.2.6. Fracture toughness K_{mat}

The resistance of material for fracture is controlled by its fracture toughness K_{mat} which finally affects the crack sizes. In the road bridges, the value is treated as Weibull distribution following the work of Lukic [23,39].

5.3. Existing fatigue test data in literature

The surface extrapolation method for structural hot spot stress and a summary of the set-ups considered are shown in Fig. 20. The tests were carried out till the failure of specimens. As the details of Nagy's tests have already been introduced in Section 2. For all the experiments, $\Delta\sigma_{HSS}$ are linearly extrapolated to the weld toe by the values at two positions ($\Delta\sigma_1$ and $\Delta\sigma_2$). The stress ranges are derived from strain measured by the gauges attached at the bottom of the deck plate except the results of Yuan [9] in which the stress ranges are calculated by the FE models. For the set-ups, the top deck plate is simply supported at the sides and fatigue loading is applied in the area between two longitudinal stiffeners, see Fig. 20b. One exception is the set-up used in Yuan [9]. The load is applied from the bottom of stiffener. It should be noted that narrow specimens are used in Yuan [9] and Li [33] with widths of 150 mm and 108 mm, respectively. For other tests, the widths of specimens range from 400 mm to 600 mm. In Table 3, the material properties of the specimens which are given by the authors in literature [8,10,33] are listed. In the current paper, only the tests results with weld penetration larger than 75% are selected and analyzed. These joints have the detail category "71" in EN1993-1-9:2006 using nominal stress approach [11]. Moreover, only the cracks initiating only from the weld toe in these tests are included. These results are grouped in the current paper for the fatigue resistance analysis using the structural hot spot stress approach.

Fig. 21a summaries the results from Bignonnet (1990) [34], Dijkstra [35], Yuan [9], Nagy [20], Li [33], under load ratio $R = -1$. In Dijkstra [35], load ratio −0.66 is used. It is grouped to $R = -1$. The fixed slope 3.00 is used in the statistical evaluation. Fatigue resistance at 2 million

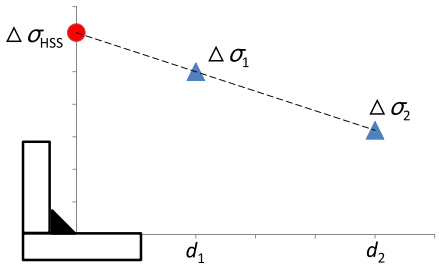

(a) Surface extrapolation approach for structural hot spot stress range calculation

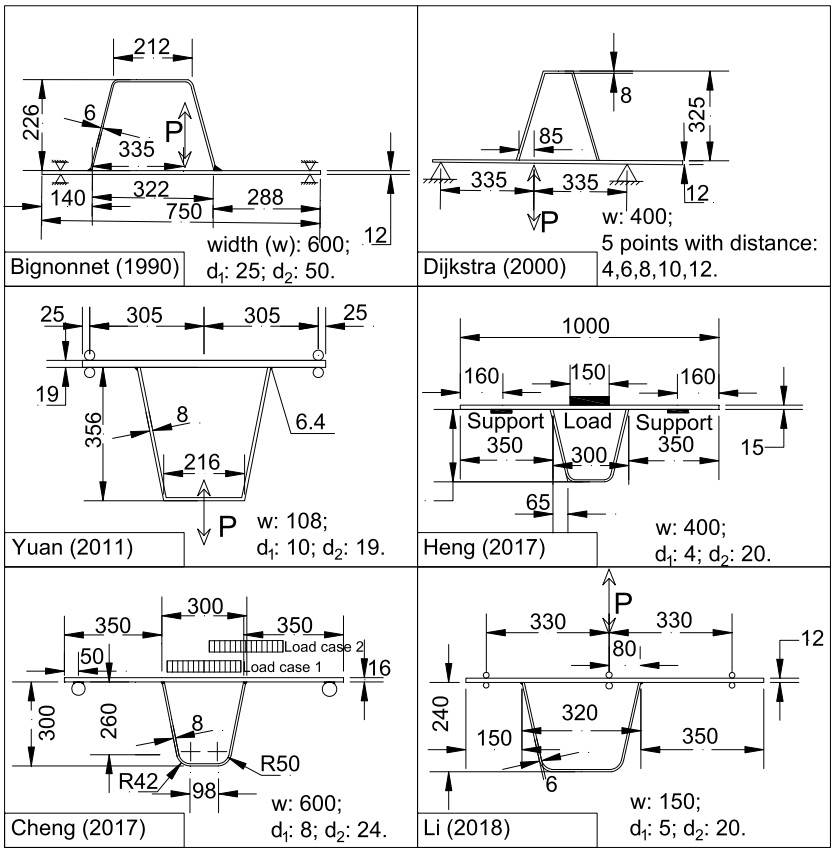

(b) Set-ups

Fig. 20. Summary of the set-ups for fatigue tests available in literature (unit: mm) [8–10,33–35].

cycles has a mean hot spot stress range (survival probability 50%) 195 MPa. For the upper (survival probability 5%) and lower bound (survival probability 95%), the stress ranges 292 MPa and 131 MPa are obtained. It should be noted that the statistical analysis with survival probability 95% on a two-sided confidence level of 75% with fixed slope 3.00 at 2 million cycles is the approach used in EN1993-1-9:2006 [11] for determining the characteristic value of detail categories under normal stress. Fatigue resistance 131 MPa can be treated as the classification of the weld toe crack based on listed experiments using hot spot stress.

Table 3
Properties of the specimens in literature [8,10,33].

Reference	σ_{yield} [MPa]	$\sigma_{ultimate}$ [MPa]
[8], 6 mm rib	400	495
[8], 16 mm deck	353	508
[10]	345	510
[33]	281	424

The results from Yuan [9], Nagy [20], Heng [8], Cheng [10] under the load ratio $R = 0$ are shown in Fig. 21b. Fatigue resistance at 2 million cycles with mean value 142 MPa is found for $R = -1$ and 0. The upper (survival probability 5%) and lower bound (survival probability 95%) are 270 MPa and 75 MPa are obtained. Fatigue resistance of the joint is affected by the load ratio R. This can be explained when recalling Paris' material parameter C with different load ratios, see Table 2. Results are thus divided into two groups, $R = -1$ and 0, in the following section analysis.

5.4. Monte Carlo simulation

For each simulation, 10^5 Monte Carlo samples are created using the aforementioned parameters. A random combination of these values is used in the calculation. Fatigue life based on the fracture mechanics

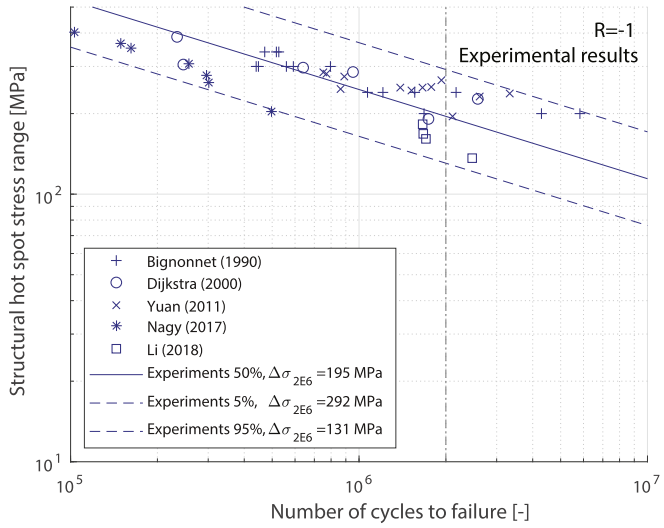

(a) $R = -1$

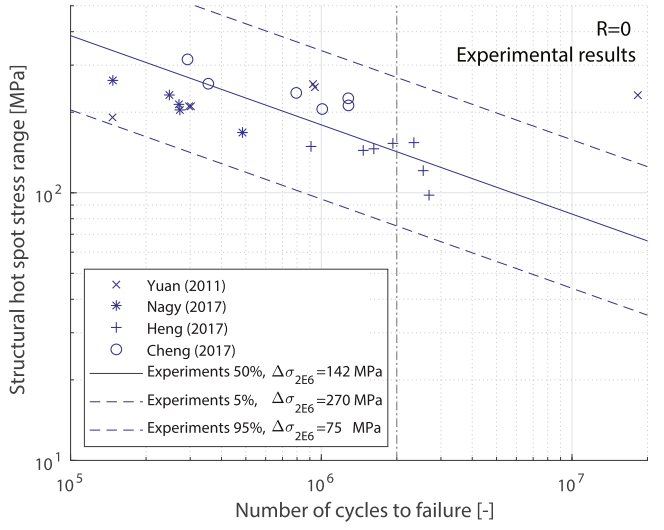

(b) $R = 0$

Fig. 21. Fatigue test results with load ratios $R = -1$ and $R = 0$ from literature.

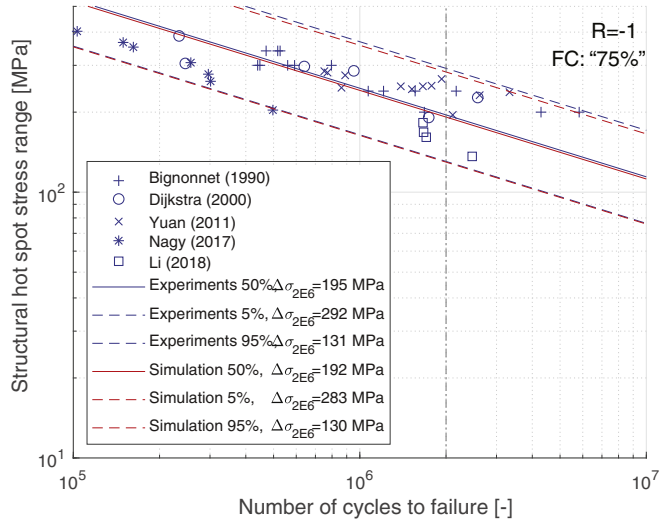

Fig. 22. Comparison of the experimental data and simulated results, $R = -1$ and FC: "75%".

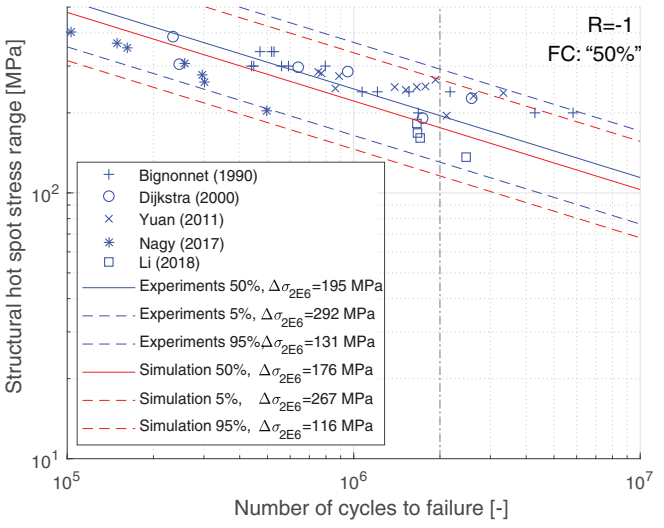

Fig. 23. Comparison of the experimental data and simulated results, $R = -1$ and FC: "50%".

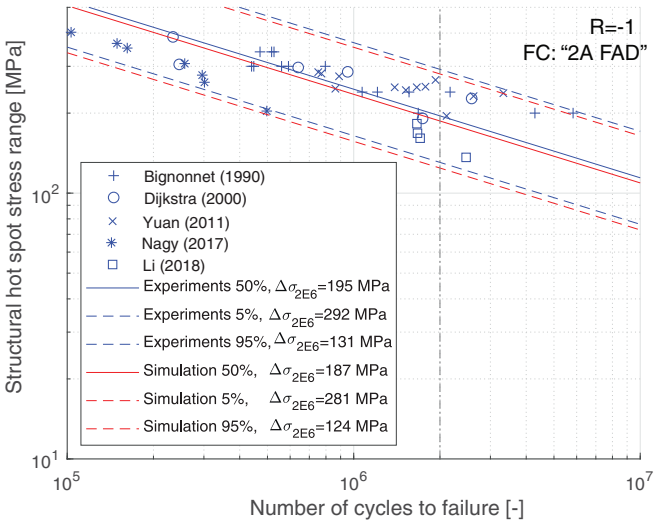

Fig. 24. Comparison of the experimental data and simulated results, $R = -1$ and FC: "2A FAD".

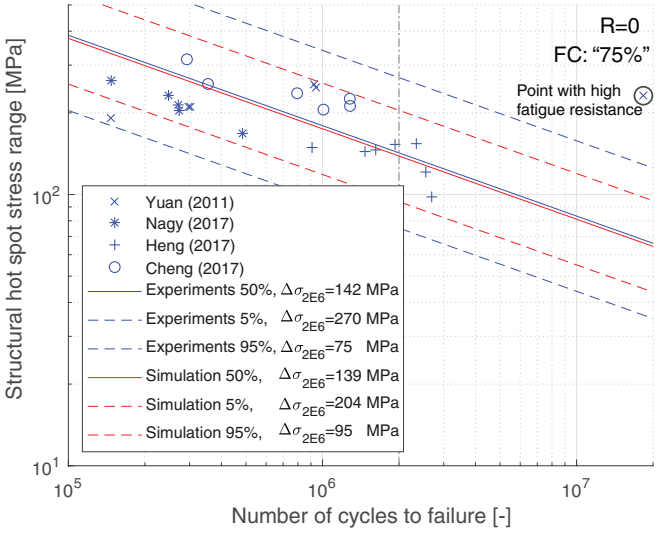

Fig. 25. Comparison of the experimental data and simulated results, $R = 0$ and FC: "75%".

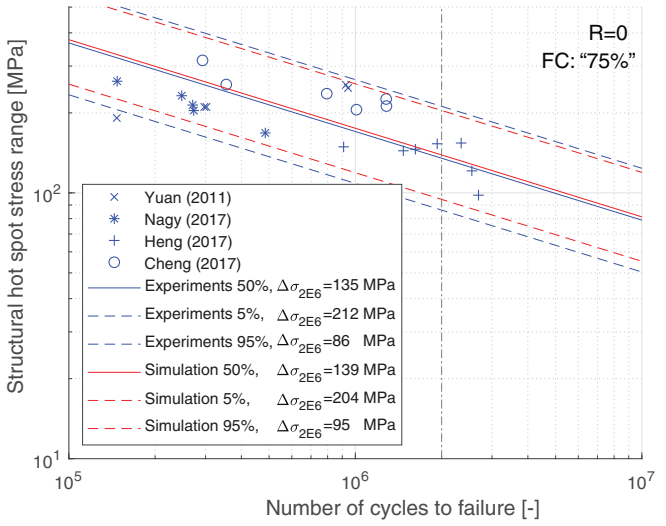

Fig. 26. Comparison of the experimental data and simulated results, $R = 0$ and FC: "75%".

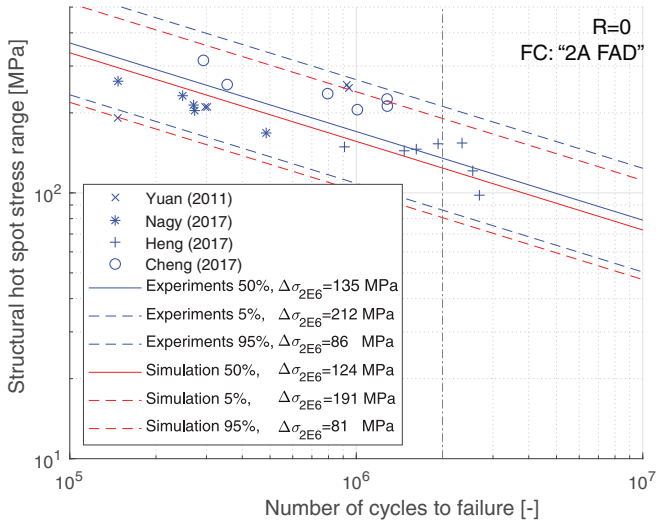

Fig. 28. Comparison of the experimental data and simulated results, $R = 0$ and FC: "2A FAD".

calculation is then obtained. The comparison between experimental data and prediction results by Monte Carlo simulation is shown from Figs. 22 to 28. The results are grouped based on the failure criteria and load ratios.

For the load ratio $R = -1$, very good agreement is found between the simulation and experiments at the mean (50%), upper (5%), and lower (95%) bound limits with failure criterion "75%". The mean stress is 192 MPa, only 3 MPa lower than the experimental value, and the differences between experimental data and simulated results are within 3% for the mean and two bound limits. The mean and characteristic values (lower bound) are the most interesting values in the fatigue assessment. These two parameters are discussed in the following sections. With failure criterion "50%", the predicted mean value from Monte Carlo simulation drops 8% (from 192 MPa to 176 MPa) compared with failure criterion "75%". The values of lower bounds decrease 11% (from 130 MPa to 116 MPa). For the "2A FAD" approach, the results are close to "75%" failure criterion with the mean value 187 MPa and lower bound value 124 MPa. The differences between "2A FAD" and "75%" are within 5%.

Figs. 25 to 28 show the results with load ratio $R = 0$. The fatigue resistance is lower than the case $R = -1$. In Fig. 25, the simulated mean value (139 MPa) is close to the experimental data (142 MPa). It should be noted that the circle black point shows very good fatigue performance from Yuan [9] and that point may cause this large deviation in statistical analysis. A comparison without that point is shown afterwards. In Fig. 26, the mean value from the experiments reduces from 142 MPa to 135 MPa. The lower bound increases from 75 MPa to 86 MPa. The prediction with failure criterion "75%" shows a good match with experimental data (difference 3% for the mean value). The deviation of experimental data is slightly larger than the simulated values (difference 10% for a lower bound). For the "2A FAD", the results are close to failure criterion "50%" (difference within 4%). It may because the structural hot spot stress range is selected with values 185 MPa and 247 MPa randomly distributed for samples in Monte Carlo simulation. The maximum stress with $R = -1$ is only half of the values in case $R = 0$. This affects the final crack sizes and the calculated fatigue resistance. The results with failure criterion "2A FAD" are close to failure criterion "75%" and failure criterion "50%" with $R = -1$ and 0, respectively.

The initial crack depth (a_0) is expected to have a big influence on fatigue life [39]. With different initial crack shapes, a_0/c_0, the crack shapes in the propagation period are different, which may affect the fatigue resistance. The effects of initial crack shape a_0/c_0 and crack depth a_0 on the fatigue resistance are presented in Figs. 29 and 30 with the failure criterion "75%". Structural hot spot stress ranges at 2 million cycles with

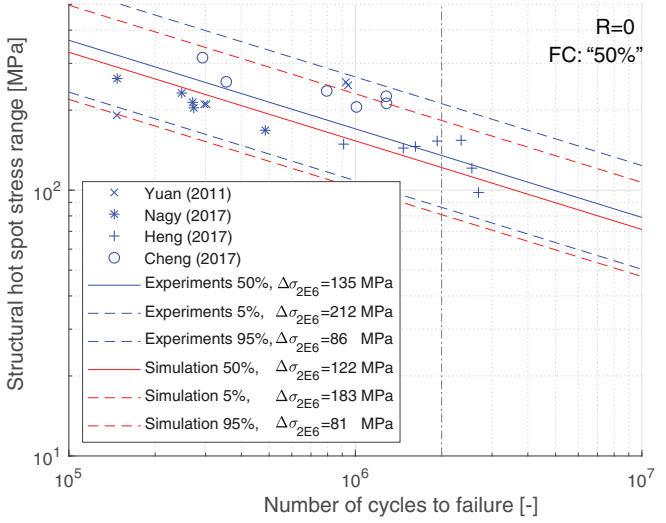

Fig. 27. Comparison of the experimental data and simulated results, $R = 0$ and FC: "50%".

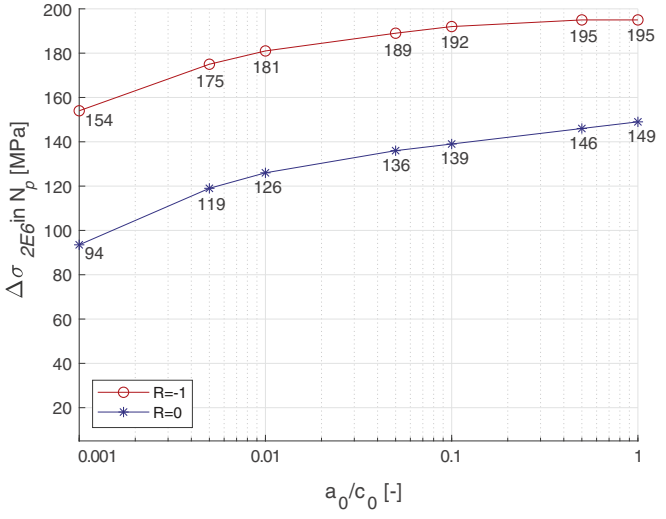

Fig. 29. Effect of initial crack shapes a_0/c_0 on the fatigue resistance, FC: "75%".

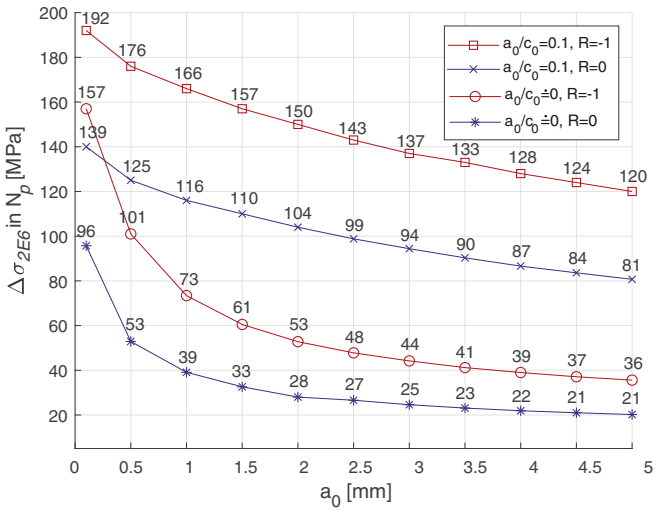

Fig. 30. Effect of initial crack depth a_0 on the fatigue resistance, FC: "75%".

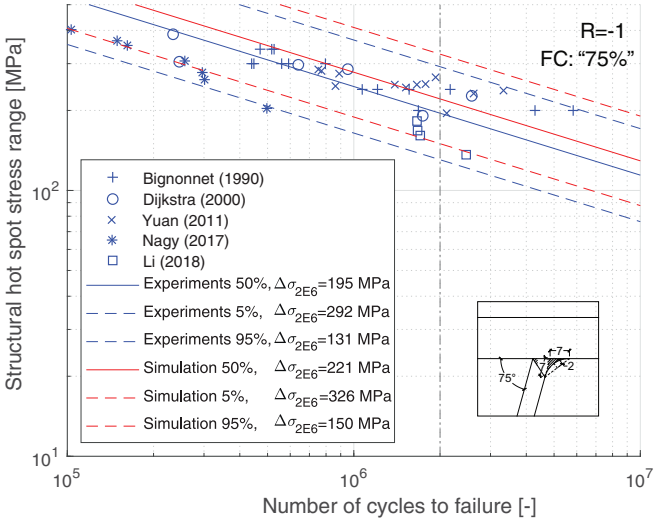

Fig. 31. Comparison of the experimental data and simulated results, Type 2 profile, $R = -1$ and FC: "75%".

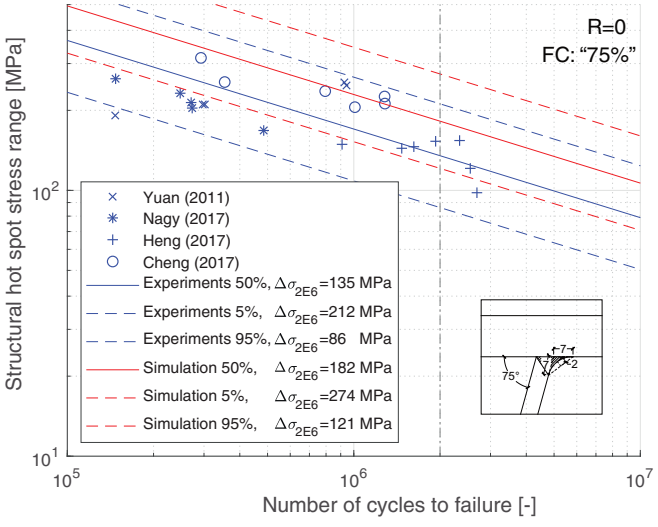

Fig. 32. Comparison of the experimental data and simulated results, Type 2 profile, $R = 0$ and FC: "75%".

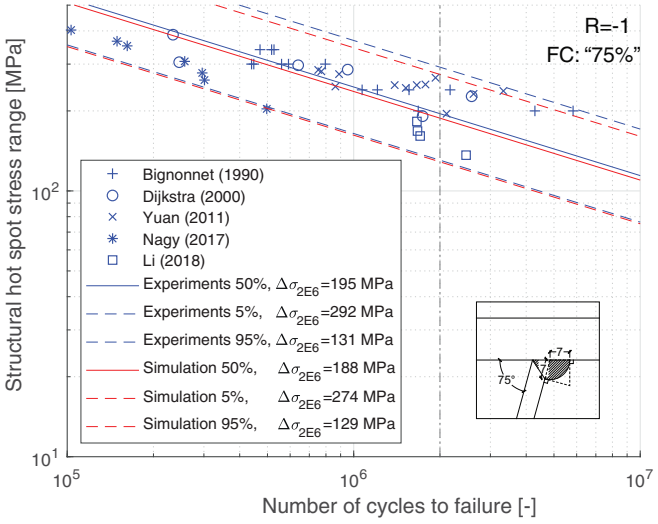

Fig. 33. Comparison of the experimental data and simulated results, Type 3 profile, $R = -1$ and FC: "75%".

survival probability 50%, $\Delta\sigma_{2E6}$, are used as the vertical axis. In the current analysis, $a_0/c_0 = 0.001$ is selected to represent the case of $a_0/c_0 \doteq 0$.

Under $R = -1$, the mean values increase from 154 MPa to 189 MPa with $a_0/c_0 = 0.001$ to $a_0/c_0 = 0.05$. It then grows with a smaller slope to 195 MPa when $a_0/c_0 = 1$. Similar trend is found at $R = 0$ while the fatigue resistance is lower.

In Fig. 30, nonlinear decreases in fatigue life with the increase of a_0. The fatigue resistances have decreased from 192 MPa to 120 MPa with a_0 increases from 0.1 mm to 5.0 mm when $R = -1$. Similar trend can be seen when $R = 0$ with $\Delta\sigma_{2E6}$ reduces from 139 MPa to 81 MPa. For the case of $a_0/c_0 \doteq 0$, a fast drop can be seen when a_0 changes from 0.1 mm to 2.0 mm. Decreases of 66% (from 157 MPa to 53 MPa) and 70% (from 96 MPa to 28 MPa) are obtained when a_0 changes from 0.1 mm to 2.0 mm under $R = -1$ and 0, respectively. The values then decrease slower till a_0=5 mm.

5.5. Effect of the weld profiles

Types 2 and 3 weld profiles, shown in Fig. 10, consider weld shape effect on the fatigue resistance of the joints.

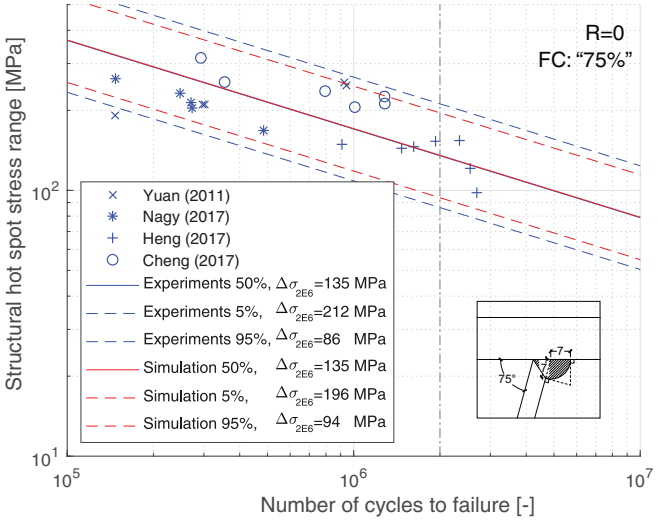

Fig. 34. Comparison of the experimental data and simulated results, Type 3 profile, $R = 0$ and FC: "75%".

In this section, probabilistic analysis is carried out for Types 2 and 3 profiles. In Figs. 31 and 32, the fatigue resistance obviously increases when the interaction angle between weld and base materials is small, with 15% (from 192 MPa to 221 MPa) and 31% (from 139 MPa to 182 MPa) increase at mean values under $R = -1$ and $R = 0$ in Monte Carlo simulation, respectively.

For the Type 3 profile with round weld toe, the values are very close to the Type 1. Under $R = -1$ and $R = 0$, the predicted mean values of fatigue resistance at 2 million are 188 MPa and 135 MPa which give a difference within 3% compared with Type 1 profile, see Figs. 33 and 34.

6. Conclusions

The fatigue crack of rib-to-deck welded joint initiating from weld toe and growing through deck plate in orthotropic steel decks is studied using linear elastic fracture mechanics. By adding the geometric correction factors M_k, which is a function of the crack size and plate thickness, to the empirical equations for a semi-ellipse crack under bending, the analytical hand calculation model can be applied for the weld toe crack propagation in the rib-to-deck joint. The following conclusions are made from this study:

- Fatigue crack propagation can be predicted by FE using multi-points extrapolation method with condition that the shape of initial crack insertion is properly assumed.
- Geometric correction factors M_k obtained by fitting the FE results with numerical functions can be added to the basic model for a crack propagation calculation model developed by Newman. Good agreement is found for the crack depth propagation when comparing the calculated values with "beach marks" from experiments.
- With shallow cracks, the simplified semi-ellipse crack propagation may cause underestimation of the crack length growth compared to the situation where intersection angles between crack front and surface at edges θ are small.
- At load ratio $R = -1$, the mean and characteristic hot spot stress ranges at 2 million cycles loading are 195 MPa and 131 MPa, respectively. For $R = 0$, the values are 142 MPa and 75 MPa. Higher load ratio loading results in lower fatigue resistance for the weld toe crack in rib-to-deck joints. It indicates that the compressive stress in the case of $R = -1$ is beneficial for fatigue resistance.
- Using the corrected model in Monte Carlo simulation, the predict mean and characteristic fatigue resistance at 2 million cycles are 192 MPa and 131 MPa with the failure criterion "75%" deck thickness and $R = -1$. For $R = 0$, the values are 135 MPa and 95 MPa, respectively. Good agreement is found between the hand calculation prediction and experimental results. For the failure criterion of "50%" deck thickness and "2A FAD", the predicted fatigue resistance is slightly lower than the case with failure criterion "75%".
- Lower fatigue resistance is found assuming the more shallow initial crack. For instance, the mean fatigue resistance at 2 million cycles reduces from 195 MPa and 154 MPa when a_0/c_0 decreases from 0.1 to 0.001 with the failure criterion "75%" and the load ratio $R = -1$.
- Fatigue resistance reduces nonlinearly with the increase of a_0. When the crack is shallow (e.g. a_0/c_0=0.001), the sharp drop is found if the initial crack depth a_0 grows from 0.1 mm to 2.0 mm. For a_0 is between the range 2.0 mm and 5.0 mm, a smaller decrease is obtained. The change is less emphasized if the crack is not so shallow (e.g. $a_0/c_0 = 0.1$).
- Weld shape profiles affect the fatigue resistance of the joint. The concave weld profile with smaller intersection angle between the weld and the base material leads to higher fatigue resistance. For example, Type 2 weld profile gives 16% higher fatigue resistance than Type 1 profile at the load ratio $R = -1$. For Type 3, 2% drop in the fatigue resistance is found compared with Type 1.

Acknowledgement

The first author would like to thank the financial support from China Scholarship Council (CSC) for the PhD study.

Appendix A. Calculation procedure of K_I using empirical equations proposed by Newman [32]

$$K_I = [M_m(\sigma_m + p_{cr}) + M_b\sigma_b]\sqrt{\frac{\pi a}{Q}} \tag{A.1}$$

where

$$Q = 1.0 + 1.464\frac{a}{c}\ \left(\frac{a}{c} <= 1\right) \tag{A.2}$$

Membrane correction factor:

$$M_m = \left[M_1 + M_2\left(\frac{a}{t}\right)^2 + M_3\left(\frac{a}{t}\right)^4\right] g f_\phi f_w \tag{A.3}$$

where

$$M_1 = 1.13 - 0.09\frac{a}{c} \tag{A.4}$$

$$M_2 = \frac{0.89}{0.2 + a/c} - 0.54 \tag{A.5}$$

$$M_3 = 0.5 - \frac{1}{0.65 + a/c} + 14\left[1 - \frac{a}{c}\right]^{24} \tag{A.6}$$

with

$$g = 1 + \left[0.1 + 0.35\left(\frac{a}{c}\right)^2\right][1 - sin(\phi)]^2 \tag{A.7}$$

the angle function for embedded elliptical-crack f_ϕ

$$f_\phi = \left[\frac{a}{c}\ cos(\phi)^2\ sin(\phi)^2\right]^{0.25} \tag{A.8}$$

the finite-width correction function

$$f_w = \left[\ sec\left(\frac{\pi c}{2b}\sqrt{\frac{a}{t}}\right)\right]^{0.5} \tag{A.9}$$

Bending correction factor:

$$M_b = M_m H \tag{A.10}$$

where the function H is developed by curve fitting

$$H = H_1 + (H_2 - H_1)\ sin(\phi)^q \tag{A.11}$$

with

$$H_1 = 1 - 0.34\frac{a}{t} - 0.11\left(\frac{a}{c}\right)()\frac{a}{t}) \tag{A.12}$$

$$H_2 = 1 + G_1\frac{a}{t} + G_2\left(\frac{a}{t}\right)^2 \tag{A.13}$$

$$q = 0.2 + \frac{a}{c} + 0.6\frac{a}{t} \tag{A.14}$$

in which

$$G_1 = -1.22 - 0.12\frac{a}{c} \tag{A.15}$$

$$G_2 = 0.55 - 1.05\left(\frac{a}{c}\right)^{0.75} + 0.47\left(\frac{a}{c}\right)^{1.5} \quad (A.16)$$

Appendix B. 2A FAD assessment in BS7910 [31,39] without considering secondary stress

The failure occurs when:

$$K_r = \left(1 - 0.14L_r^2\right)\left(0.3 + 0.7e^{-0.65L_r^6}\right) \quad \text{if} \quad L_r \le L_{r,max} \quad (B.1)$$

$$K_r = 0 \quad \text{if} \quad L_r > L_{r,max} \quad (B.2)$$

where:

$$K_r = K/K_{mat} \quad (B.3)$$

$$L_{r,max} = \frac{min\left[1.2\sigma_y, 0.5\left(\sigma_y + \sigma_u\right)\right]}{\sigma_y} \quad (B.4)$$

For surface flaws in plates under bending:

$$\sigma_{ref} = \frac{2Pb}{3(1-a'')^2} \quad (B.5)$$

in which:

$$a'' = \frac{a}{t}\left[1 + \left(\frac{a}{c}\right)^{-1}\right] \quad if \quad w > 2(c+t) \quad (B.6)$$

$$a'' = \frac{2a}{t}\frac{c}{w} \quad if \quad w < 2(c+t) \quad (B.7)$$

Note: w is the half width of the plate.

References

[1] R. Connor, J. Fisher, Manual for Design, Construction, and Maintenance of Orthotropic Steel Deck Bridges, Federal Highway Administration, 2012.
[2] M.H. Kolstein, Fatigue Classification of Welded Joints in Orthotropic Steel Bridge Decks, Doctoral Dissertation Delft University of Technology, Delft, Netherlands, 2007.
[3] F. De Jong, Renovation Techniques for Fatigue Cracked Orthotropic Steel Bridge Decks, Doctoral Dissertation Delft University of Technology, Delft, Netherlands, 2007.
[4] S. Kainuma, M. Yang, Y.-S. Jeong, S. Inokuchi, A. Kawabata, D. Uchida, Experiment on fatigue behavior of rib-to-deck weld root in orthotropic steel decks, J. Constr. Steel Res. 119 (2016) 113–122.
[5] P.A. Tsakopoulos, J.W. Fisher, Full-scale fatigue tests of steel orthotropic decks for the Williamsburg bridge, J. Bridg. Eng. 8 (5) (2003) 323–333.
[6] S. Ya, K. Yamada, T. Ishikawa, Fatigue evaluation of rib-to-deck welded joints of orthotropic steel bridge deck, J. Bridg. Eng. 16 (4) (2010) 492–499.
[7] Q. Zhang, Y. Liu, Y. Bao, D. Jia, Y. Bu, Q. Li, Fatigue performance of orthotropic steel-concrete composite deck with large-size longitudinal ushaped ribs, Eng. Struct. 150 (2017) 864–874.
[8] J. Heng, K. Zheng, C. Gou, Y. Zhang, Y. Bao, Fatigue performance of ribto- deck joints in orthotropic steel decks with thickened edge u-ribs, J. Bridg. Eng. 22 (9) (2017), 04017059.
[9] H. Yuan, Optimization of Rib-to-Deck Welds for Steel Orthotropic Bridge Decks, Masters Thesis Virginia Polytechnic Institute and State University, Blacksburg, Virginia, the United States, 2011.
[10] B. Cheng, X. Ye, X. Cao, D. Mbako, Y. Cao, Experimental study on fatigue failure of rib-to-deck welded connections in orthotropic steel bridge decks, Int. J. Fatigue 103 (2017) 157–167.
[11] EN1993-1-9, Design of Steel Structures-General-Part 1.9: Fatigue Strength of Steel Structure, European Committee for Standardization, Brussels, 2006.
[12] AASHTO, AASHTO LRFD Bridge Design Specifications, 7th edition American association of state highway and transportation officials, Washington, DC, 2014.
[13] JRA, Fatigue Design Guidelines for Steel Highway Bridges, Japan Road Association, Tokyo, 2002 (in Japanese).
[14] A. Hobbacher, et al., Recommendations for Fatigue Design of Welded Joints and Components, Springer International Publishing, 2016.
[15] A. Kanvinde, Predicting fracture in civil engineering steel structures: state of the art, J. Struct. Eng. 143 (3) (2017), 03116001.
[16] J. Lewandowski, D. Rozumek, Cracks growth in S355 steel under cyclic bending with fillet welded joint, Theor. Appl. Fract. Mech. 86 (2016) 342–350.
[17] M. Aygül, M. Al-Emrani, Z. Barsoum, J. Leander, Investigation of distortion-induced fatigue cracked welded details using 3d crack propagation analysis, Int. J. Fatigue 64 (2014) 54–66.
[18] M. Aygül, M. Al-Emrani, Z. Barsoum, J. Leander, An investigation of distortion-induced fatigue cracking under variable amplitude loading using 3d crack propagation analysis, Eng. Fail. Anal. 45 (2014) 151–163.
[19] R. Brighenti, A. Carpinteri, Surface cracks in fatigued structural components: a review, Fatigue Fract. Eng. Mater. Struct. 36 (12) (2013) 1209–1222.
[20] W. Nagy, Fatigue Assessment of Orthotropic Steel Decks Based on Fracture Mechanics, Doctoral Dissertation Gent University, Ghent, Belgium, 2017.
[21] R.F. Sanches, A.M. De Jesus, J.A. Correia, A. Da Silva, A. Fernandes, A probabilistic fatigue approach for riveted joints using Monte Carlo simulation, J. Constr. Steel Res. 110 (2015) 149–162.
[22] J.A. Correia, A.M.D. Jesus, A. Fernández-Canteli, Local unified probabilistic model for fatigue crack initiation and propagation: application to a notched geometry, Eng. Struct. 52 (2013) 394–407.
[23] M. Lukic, C. Cremona, Probabilistic optimization of welded joints maintenance versus fatigue and fracture, Reliab. Eng. Syst. Saf. 72 (3) (2001) 253–264.
[24] J. Maljaars, E. Bonet, R. Pijpers, Fatigue resistance of the deck plate in steel orthotropic deck structures, Eng. Fract. Mech. 201 (2018) 214–228.
[25] T.L. Anderson, Fracture Mechanics: Fundamentals and Applications, CRC press, 2005.
[26] P. Paris, F. Erdogan, A critical analysis of crack propagation laws, J. Basic Eng. 85 (4) (1963) 528–533.
[27] J.R. Rice, A path independent integral and the approximate analysis of strain concentration by notches and cracks, J. Appl. Mech. 35 (2) (1968) 379–386.
[28] J. Yau, S. Wang, H. Corten, A mixed-mode crack analysis of isotropic solids using conservation laws of elasticity, J. Appl. Mech. 47 (2) (1980) 335–341.
[29] Abaqus, Systèmes Dassault, Abaqus Analysis User's Manual, Dassault Systèmes Simulia, 2014.
[30] FRANC3D, Fracture Analysis Consultants, FRANC3D V7.1 ABAQUS Tutorial, Fracture Analysis Consultants, Inc, 2017.
[31] BSI, BS 7910:2013+A1:2015: Guide to Methods for Assessing the Acceptability of Aws in Metallic Structures, British Standards Institution, London, 2015.
[32] J.C. Newman Jr., I.S. Raju, An empirical stress-intensity factor equation for the surface crack, Eng. Fract. Mech. 15 (1–2) (1981) 185–192.
[33] M. Li, Y. Suzuki, K. Hashimoto, K. Sugiura, Experimental study on fatigue resistance of rib-to-deck joint in orthotropic steel bridge deck, J. Bridg. Eng. 23 (2) (2018), 04017128.
[34] A. Bignonnet, B. Jacob, J. Caracilli, M. LaFrance, Fatigue resistance of orthotropic steel decks, Proceedings IABSE Workshop Remaining Fatigue Life of Steel Structures, Lausanne, Switzerland 1990, pp. 227–236.
[35] O.D. Dijkstra, T. Nicolaas, Vermoeiingsonderzoek Reparatiemethode Trog Dekplaat Verbindingen Moerdijkbrug, TNO Report 2000-CON-R4016, TNO Bouw, Rijswijk, The Netherlands, 2000 (In Dutch).
[36] P. Warzynek, B. Carter, L. Banks-Sills, The M-integral for computing stress intensity factors in generally anisotropic materials, NASA Consult. Rep. (2005) (NASA/CR—2005–214006, 88 pages).
[37] X. Lin, R. Smith, Finite element modelling of fatigue crack growth of surface cracked plates: part II: crack shape change, Eng. Fract. Mech. 63 (5) (1999) 523–540.
[38] U. Zerbst, R. Ainsworth, H.T. Beier, H. Pisarski, Z. Zhang, K. Nikbin, T. Nitschke-Pagel, S. Münstermann, P. Kucharczyk, D. Klingbeil, Review on fracture and crack propagation in weldments – a fracture mechanics perspective, Eng. Fract. Mech. 132 (2014) 200–276.
[39] M. Lukic, et al., Bridge fatigue guidance - meeting sustainable design and assessment, Europen Commission Technical Report, 2013.